# Impact of the nanostructuration on the chemical composition of nickel oxide nanoparticles

Baptiste Polteau,[†,‡] François Cheviré,[†] Franck Tessier,[†] Philippe Deniard,[‡] Eric Gautron,[‡] Laurent Cario,[‡] and Stéphane Jobic[‡]

[†] Univ Rennes, CNRS, ISCR (Institut des Sciences Chimiques de Rennes) - UMR 6226, F-35000 Rennes, France

[‡] Institut des Matériaux Jean Rouxel (IMN), Université de Nantes, CNRS, 2 rue de la Houssinière, BP 32229, 44322 Nantes cedex 03, France

## Supporting Information

### *Experimental section*

***Synthesis.*** NiO materials were synthesized by thermal decomposition of $Ni_3O_2(OH)_4$.[1] Practically, 800 mg of the precursor were placed in an alumina crucible and then heated for 2 hours in a muffle furnace in air at temperatures ranging from 250 and 900 ° C (heating rate = 10°C/min). Samples were cooled down to room temperature by turning off the oven, and then stored in the desiccator with KOH. Hereafter samples labelled NiO-T refer as to materials prepared at the synthesis temperature T (°C). For T in the 250-500 °C and 500-800 °C ranges, materials were black and grey, respectively. Above 800 ° C, NiO is greenish as expected for the 1:1 stoichiometry.

***X-ray diffraction***. In situ temperature X-Ray diffraction patterns were recorded for 2h in the 10-90° 2θ range with a 0.008° step on a Bruker D8 Advance diffractometer (Cu K-L2,3 radiation, LinxEye detector) equipped with a XRK 900 Anton Paar reactor chamber. Data were collected at 30°C, then from 50 °C to 700 °C every 50 °C with a 10°C.min$^{-1}$ heating rate. Room temperature X-Ray diffraction patterns for the microstructural analysis were recorded in the 5-120° 2θ range with a 0.026° step and 400 s by step on a Panalytical X'PERT Powder diffractometer (Cu K-L2,3 radiation, 40 kV, 40 mA, PixCell1D detector). All phase analyses were performed using the HighScore Plus software and all data refinements were carried out with the Fullprof suite software[2] taking into account both crystallite size and strains for the peak broadening.

***Electron microscopy***. Transmission electron microscopy (TEM) analyses were realized on a Hitachi H9000NAR (300 kV, Scherzer resolution 0.18 nm) microscope. Photographs were used to determine the grain size distribution. In that context, particle diameters were measured manually on several TEM shots using the ImageJ processing software. In order to get good statistics, measurements on more than 100 particles were carried out (on a large series of photographs), and results fitted via a normal curve to access to the mean particle size. The distribution of particle sizes was also represented as a histogram.

***Specific surface area measurements.*** The Brunauer-Emmet-Teller (BET) specific surface area measurements were carried out with a Micromeritics FlowSorb II 2300 instrument using a mixture of $N_2$/He (30%/70%). To avoid the surface hydration, samples were previously degassed under dynamic gas flow ($N_2$/He) at 100-110 °C.

***Thermal analyses.*** Thermogravimetric and differential thermal analyses (TGA/DTA) measurements were carried out with a TA SDT 2960 instrument. Data were collected from room temperature to 800 °C with a heating rate of 10 °C/min in air atmosphere.

***Mass spectroscopy.*** Mass spectroscopy analysis (MS) were realized with a Omnistar™ from Pfeiffer Vacuum and coupled with the thermal analyses. Experimental conditions are identical to the thermal TGA/DTA measurements.

***Density measurements***. The Micromeritics AccuPyc 1330 system was used for density measurements by pycnometry under He pressure. To avoid any surface hydration, the density measurements were realized on dried sample after the specific surface area analyses.

***Chemical analyses.*** Oxygen contents were determined with a Leco TC-600 analyzer using the inert gas fusion method where oxygen is detected as $CO_2$ by infrared detection.

***Magnetic measurements.*** A Quantum Design SQUID magnetometer (MPMS XLS 5) was used for the magnetic measurements on the powder samples. The data were collected at RT under a magnetic field ranging from 0 to 5 Tesla, and at 0.5 Tesla in the 2-20 K temperature range

***Practical information***

***Details about the thermal decomposition $Ni_3O_2(OH)_4$ into NiO (see Figures S1 and S2):*** The *in situ* thermal decomposition of $Ni_3O_2(OH)_4$ into NiO was followed by X-ray diffraction in the 20-700 °C temperature domain (**Figure S1**). From room temperature to 100 °C, only characteristic peaks of the poorly crystallized $Ni_3O_2(OH)_4$ precursor are detected. From *ca.* 150 °C, $Ni_3O_2(OH)_4$ starts to decompose into NiO. The phase transformation is complete at 200 °C where only a single NiO phase is detected by XRD. This decomposition behavior agrees well with TGA and DTA measurements (**Figure S2**) that present a weight lost around 12% in the 100-220 °C temperature range associated to the dehydration of the precursor according to the $Ni_3O_2(OH)_4 \rightarrow 4Ni_{0.75}O + 2H_2O$ reaction. From 200 to 700 °C, the width of the diffraction peaks continuously decreases suggesting a continuous increase of the crystallite size (CS) with temperature. This would go along with a constant modification of the chemical composition from *ca.* $Ni_{0.75}O$ at T=200 °C to NiO at T=800 °C with a progressive weight loss due to oxygen release (**Figure S2**). To confirm this assertion a comprehensive study was perform on NiO-T samples.

***Methodology used to determine the thickness e of the Ni-deficient layer in model 1 (see Figure S5)***: The core density is approximated to that of bulk NiO, i.e. 6.81 g/cm$^3$, and the shell density to that of an hypothetical oxygen close shell packing, i.e. 1.46 g/cm$^3$ , i.e. NiO structure without Ni. The calculated density can then written $\rho_{calc} = (1.46\times(R^3-(R-e)^3)+6.81\times(R-e)^3)/R^3$ and, in the approximation of spherical and monodispersed particles, the specific surface area can be determined from SSA = $6/\rho_{calc}\times 2R$. The thickness of the top-layer is estimated between 1.3 Å and 2.5 Å depending on whether the density evolution is fitted versus the crystallite size or the specific surface area of the NiO-T samples.

***Methodology followed to extract the corrected particle volume in model 2 (see Figure 4):*** As the volume of an octahedron is 3 times smaller than the one of a sphere with a diameter equal to its diagonal, direct comparison of the data obtained from the octahedral model to the experimental data

corresponding to more spherical particles leads to discrepancies due to the important difference in quantity of matter involved. In order to better confront the octahedral model to the experimental results and compare similar amount of matter, the calculated particle size is then approximated to the one of a sphere with a volume equivalent to that of the octahedral particle. Its diameter is then slightly smaller than the apical distance of the associated octahedron as schemed in the inset of **Figure 4b** (see also **Table S3**). To reach such equivalence, the sphere diameter has to be defined as $\varnothing_{sphere} = 2\times(3\times V_{oct.}/4\pi)^{1/3}$ with $V_{oct}$ defined as $(\varnothing_{oct.})^3 / 6$.

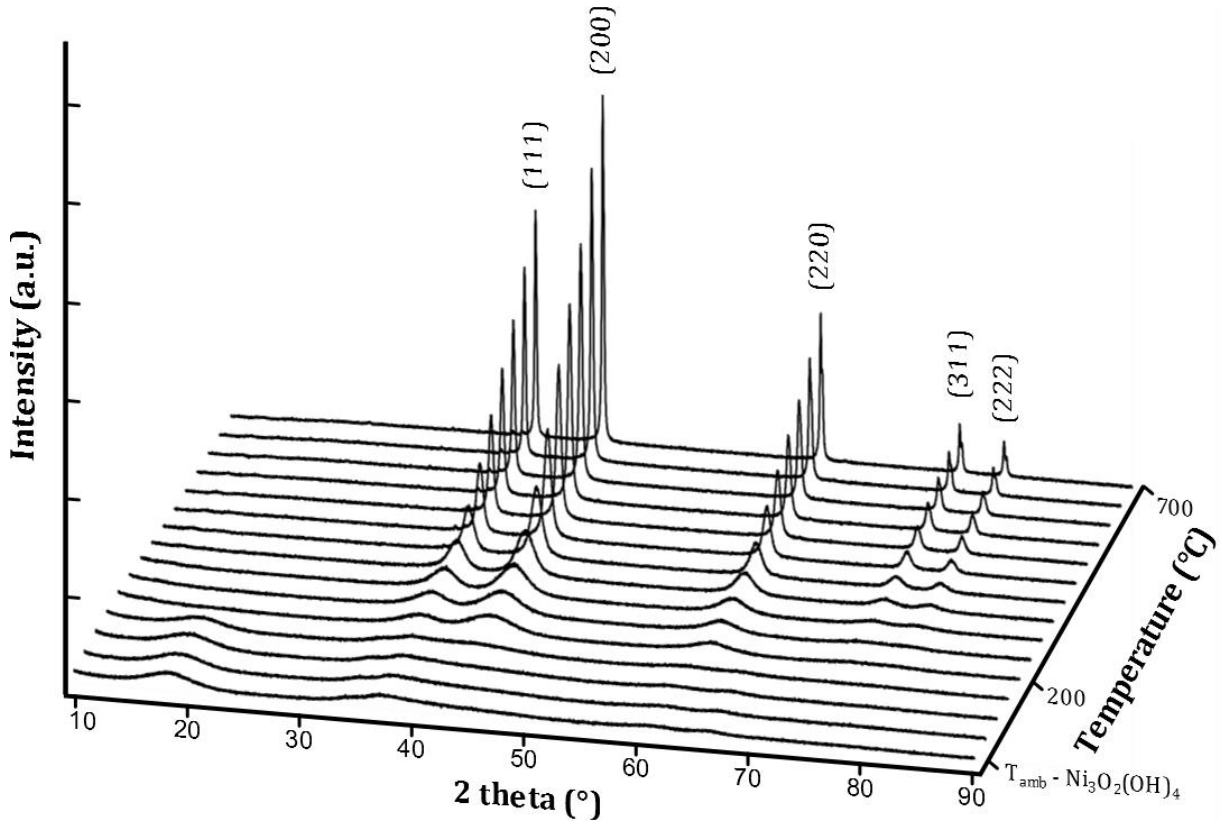


**Figure S1**. Thermal decomposition of $Ni_3O_2(OH)_4$ into NiO followed by X-ray diffraction. Data were collected by step of 50°C.

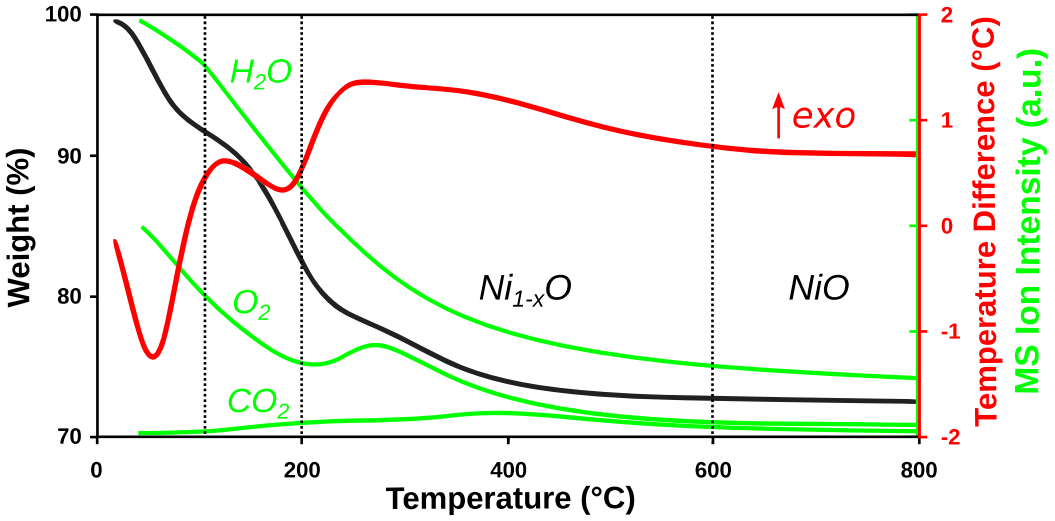


**Figure S2**. Thermal analyses (TGA/DTA/MS) for $Ni_3O_2(OH)_4$.

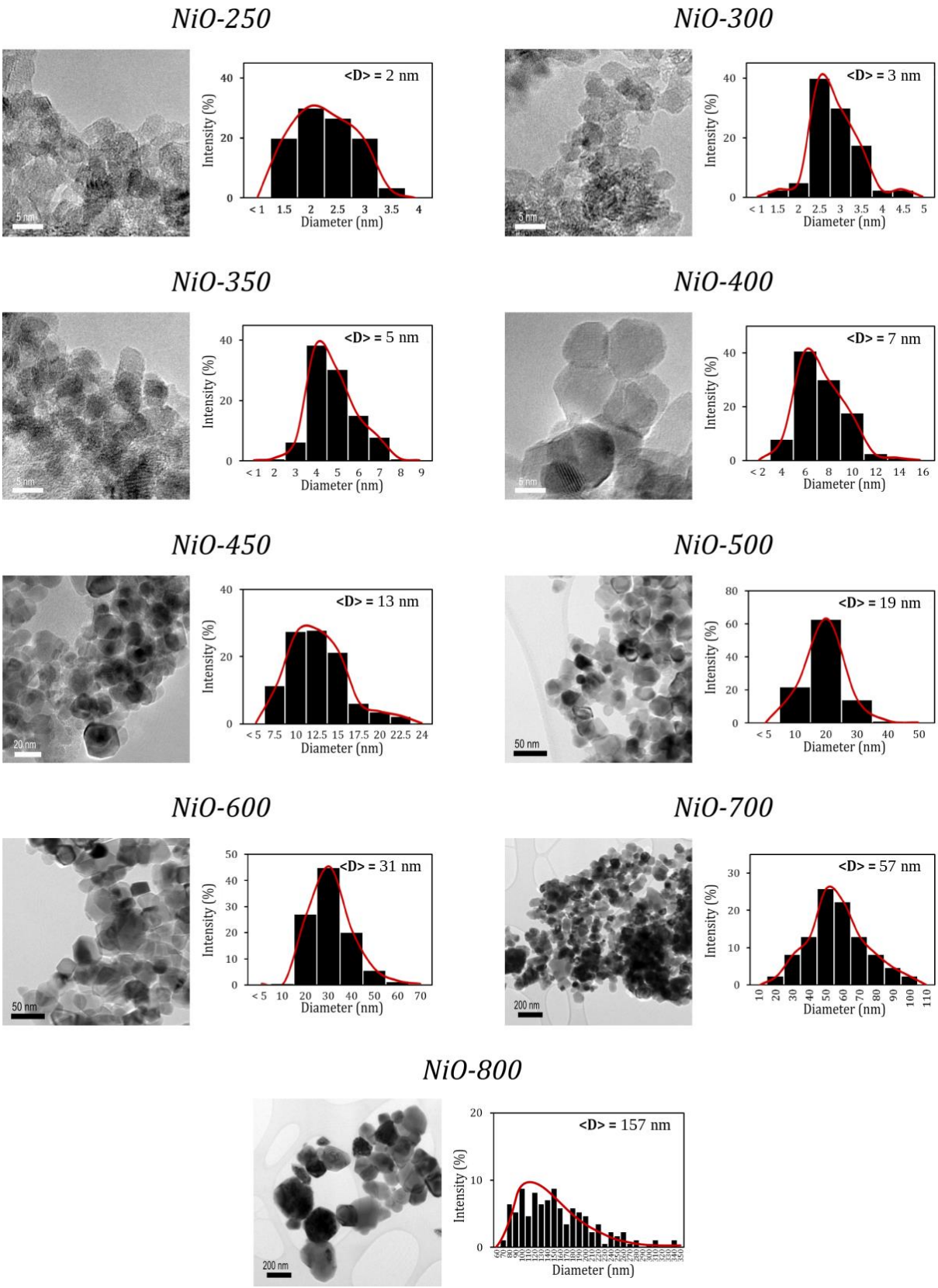


**Figure S3**. Transmission electron microscopy micrographs, distribution of particle size and average particle sizes (<D>) of NiO-T samples. The average particle diameter <D> was obtained from the analysis of more than 100 particles per sample from different photographs. Only one photograph per sample is given here.

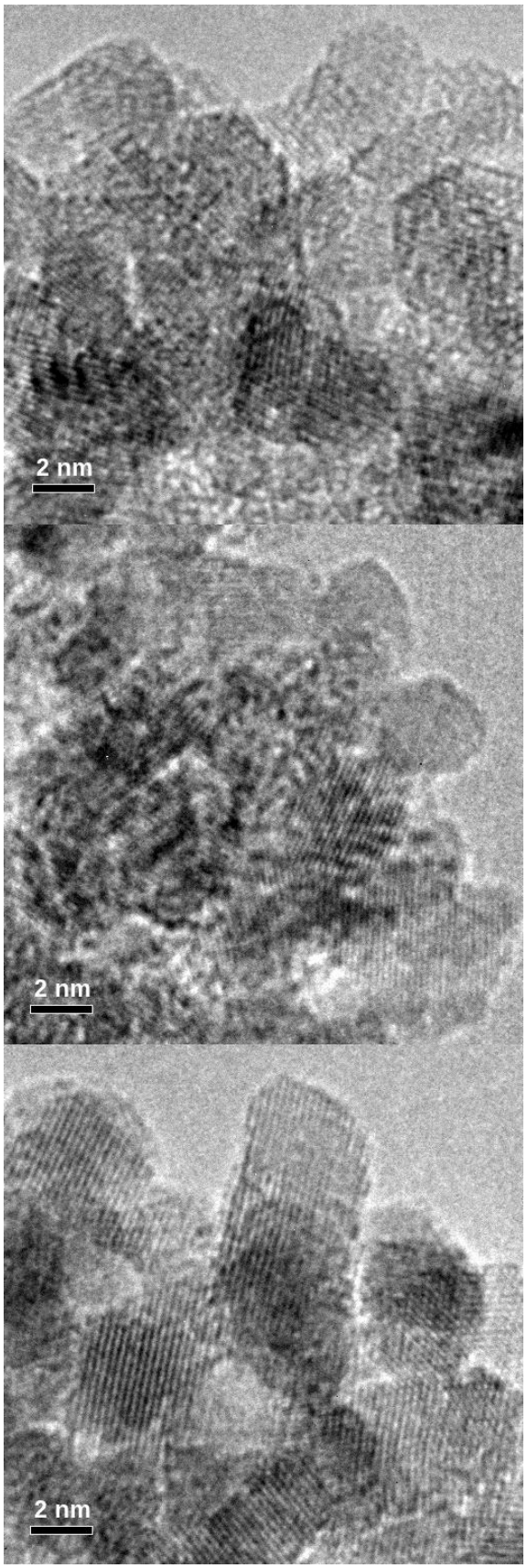


**Figure S4**. Zoom of NiO-250 (top), NiO-300 (middle) and NiO-350 (bottom) images of Figure S3 illustrating the good crystallinity of prepared materials

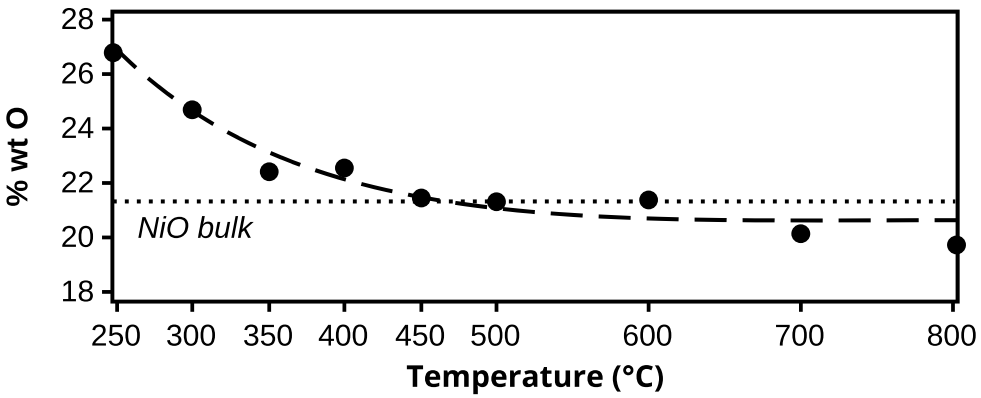


**Figure S5**. Oxygen analysis for the samples annealed for 2h in air at different temperatures from 250 °C to 800 °C.

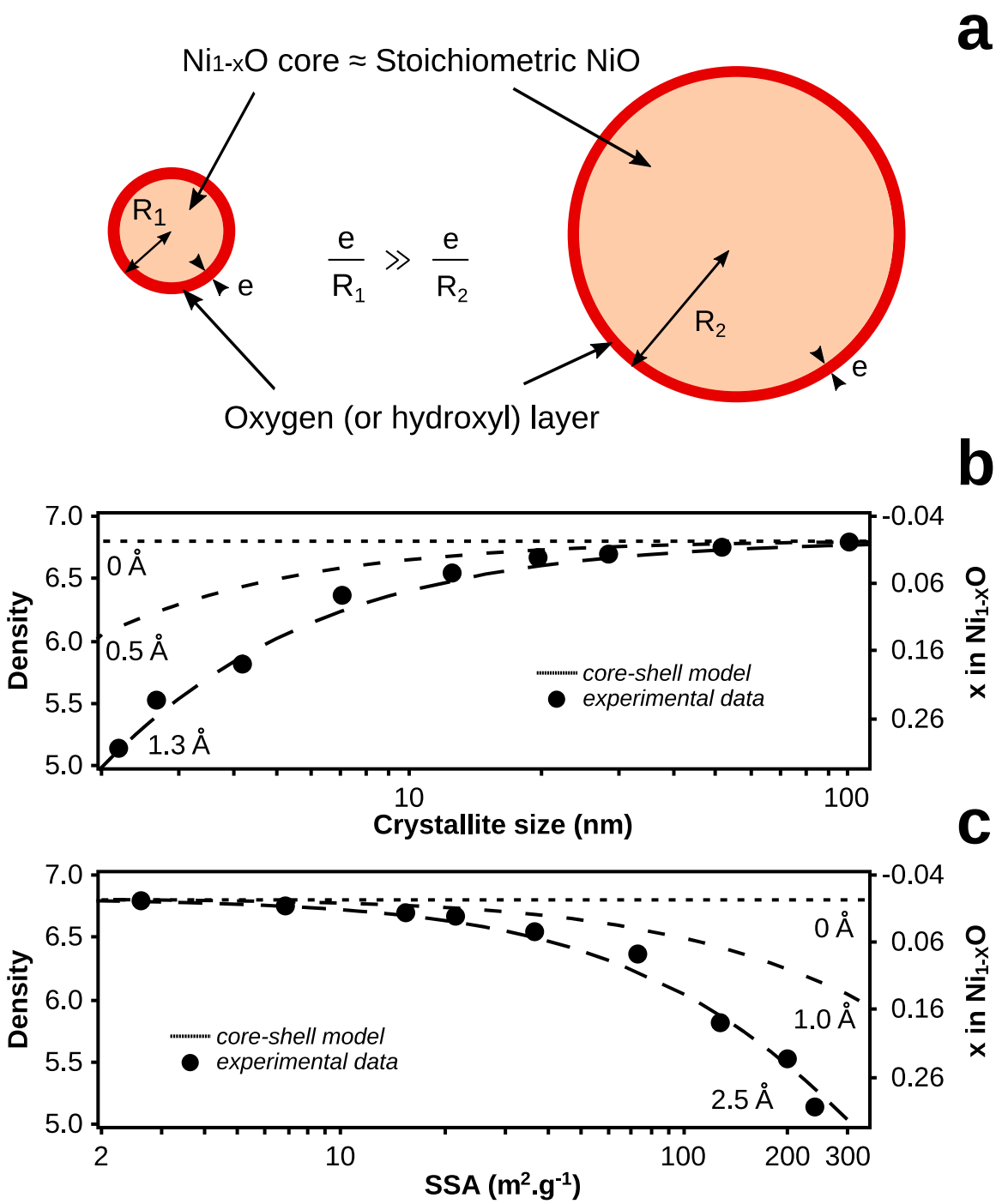


**Figure S6**. Evolution of the density as a function of the particle size (2R) or the specific surface area with different oxygen layer thicknesses.

**Table S1.** Specific surface area (SSA), crystallite sizes (CS) and particle sizes for all NiO-T samples annealed for 2h in air at 250°C < T < 800°C.

| *Temperature (°C)* | *SSA ($m^2/g$)* | *Crystallite sizes (nm)* | *Particle sizes (nm)* |
|---|---|---|---|
| 250 | 240 | 2 | 2 |
| 300 | 200 | 3 | 3 |
| 350 | 128 | 4 | 5 |
| 400 | 73 | 7 | 7 |
| 450 | 37 | 14 | 13 |
| 500 | 22 | 22 | 19 |
| 600 | 16 | 32 | 31 |
| 700 | 7 | 66 | 57 |
| 800 | 3 | 193 | 157 |

**Table S2.** Oxygen analysis, density measurements, Ni off-stoichiometry and refined cell volume for all NiO-T samples annealed for 2h in air at 250°C < T < 800°C.

| *Temperature (°C)* | *wt. O (%)* | *Density* | *x in $Ni_{1-x}O$* | *Refined cell volume ($Å^3$)* |
|---|---|---|---|---|
| 250 | 26.8(9) | 5.14(3) | 0.30 | 73.09(11) |
| 300 | 24.7(5) | 5.52(2) | 0.23 | 73.29(6) |
| 350 | 22.5(6) | 5.82(4) | 0.18 | 73.06(2) |
| 400 | 22.6(9) | 6.37(1) | 0.08 | 72.92(1) |
| 450 | 21.4(3) | 6.55(1) | 0.05 | 72.88(1) |
| 500 | 21.2(8) | 6.67(2) | 0.03 | 72.89(1) |
| 600 | 21.4(2) | 6.69(3) | 0.02 | 72.88(1) |
| 700 | 20.2(1) | 6.75(3) | 0.01 | 72.92(1) |
| 800 | 19.6(3) | 6.80(2) | 0.00 | 72.96(1) |

**Table S3.** Detailed calculations for the atomistic approach based on the growth model of a $[NiO_6]$ octahedron.

| ***n*** | ***Nb At. (O)*** | ***Nb At. (Ni)*** | ***Octahedron diagonal (nm)*** | ***Calculated density*** | ***% Off-stoichiometry (Ni)*** | ***Isovolumic sphere diameter (nm)*** |
|---|---|---|---|---|---|---|
| 2 | 6 | 1 | **0.81** | **2.86** | **83.3** | **0.56** |
| 4 | 44 | 19 | **1.65** | **4.04** | **56.8** | **1.13** |
| 6 | 146 | 85 | **2.48** | **4.76** | **41.8** | **1 .70** |
| 8 | 344 | 231 | **3.32** | **5.19** | **32.8** | **2.27** |
| 10 | 670 | 489 | **4.16** | **5.47** | **27.0** | **2.84** |
| 12 | 1156 | 891 | **4.99** | **5.67** | **22.9** | **3.41** |
| 14 | 1834 | 1469 | **5.83** | **5.82** | **19.9** | **3.98** |
| | | | ⋮ | | | |
| 242 | $94.10^5$ | $93.10^5$ | **100.7** | **6.75** | **1.2** | **69.0** |
| | | | ⋮ | | | |
| 960 | $59.10^7$ | $59.10^7$ | **401.0** | **6.79** | **0.3** | **273.8** |

- Octahedron diagonal is expressed as $\varnothing_{oct.} = 2(n-1) \times [r(Ni^{2+}) + r(O^{2-})] + 2\sqrt{2} \times r(O^{2-})$ with $R(Ni^{2+}) = 0.69$ Å and $R(O^{2-}) = 1.40$ Å for even n (O terminal surfaces).
- $\rho_{calc} = (N_O \times 15.9994 + N_{Ni} \times 58.693) / N_A \times 1/V_{oct.}$ where $N_O$, $N_{Ni}$ are the number of Oxygen and Nickel atoms in the octahedron-like nanoparticles, $N_A$ the Avogadro number, and Voct the volume of the octahedron-like nanoparticle ($V_{oct} = (\varnothing_{oct.})^3 / 6$).
- The off-stoichiometry percentage towards a 1:1 Ni:O ideal stoichiometry is given by the equation: $Off._{Ni}\% = (1 - N_{Ni}/N_O) \times 100$.

(1) Polteau, B.; Tessier, F.; Cheviré, F.; Cario, L.; Odobel, F.; Jobic, S. Synthesis of Ni-poor NiO Nanoparticles for p-DSSC Applications. *Solid State Sci.* **2016**, 54, 37-42.

(2) Rodriguez-Carvajal, J. Recent Advances in magnetic structure determination by neutron powder diffraction. *Physica B.* **1993**, 192, 55-69.